Materials Advances

ROYAL SOCIETY OF CHEMISTRY

PAPER

View Article Online
View Journal | View Issue

Cite this: *Mater. Adv.*, 2022, 3, 5375

Received 21st March 2022,
Accepted 29th April 2022

DOI: 10.1039/d2ma00324d

rsc.li/materials-advances

Superconductivity in Bi based Bi_2PdPt

A. Kataria, T. Agarwal, S. Sharma, D. Singh, S. Marik and R. P. Singh *

We report the synthesis and properties of superconducting Bi_2PdPt, a new member of the Bi–Pd based compounds that are known for simultaneous existence of topological surface states and superconductivity. It crystallizes in a hexagonal structure having space group $P6_3/mmc$. A detailed investigation of the properties *via* transport, magnetization and specific heat measurements confirms bulk superconductivity with a transition temperature, T_C, of 4.0 (1) K in the moderate coupling limit.

I. Introduction

The topological aspects of electronic states provide a thrust in the recent research of condensed matter physics. With the realization of spin polarization in these electronic states, various exotic quantum phases emerge, such as topological insulators, topological semimetals, and topological superconductors (TSCs).[1–3] Particularly, topological superconductors have attracted immense attention because of the potential appearance of exotic quasiparticles called Majorana fermions and their application in topological quantum computing. A topological superconductor is characterized by a bulk superconducting gap and Majorana zero modes at the symmetry protected topological surface states (TSSs).[3] The various proposed ways to realize a TSC include carrier doped topological insulator and superconductor–topological insulator heterostructures,[4–6] which introduce the challenge of preparing high-quality samples and observing interfacial phenomena. Here, the bulk compounds having topological nontrivial band structure and superconductivity coexist intrinsically emerge as a promising route to realize topological superconductivity.

Bi-based materials are well known for the presence of TSSs.[7–14] And Bi-based binary systems α-PdBi, α-$PdBi_2$, and β-$PdBi_2$ are among the promising candidates exhibiting bulk topological superconductivity. Notably, in α-$PdBi_2$ and non-centrosymmetric α-PdBi, Rashba surface states near the Fermi level, E_F, were theoretically predicted and experimentally verified *via* angle-resolved photoemission spectroscopy (ARPES) with intrinsic superconductivity.[15–20] Moreover, the observed non-helical spin texture near E_F for β-$PdBi_2$ combined with the various reports of fully gapped multiband superconductivity in bulk suggests the possible presence of Majorana fermions at the surface states.[21–25]

Recently, $PtBi_2$ has been shown to exhibit a large anisotropy for in-plane and inter-plane transport and stated as a bulk topological metal with pressure-induced superconductivity at 2.0 K.[26,27] This indicates that the vast family of Bi compounds is associated with various aspects of nontrivial topological electronic states and this is accompanied by superconductivity, which demands a detailed investigation in the respective family. Furthermore, the spin–orbit coupling (SOC) strength affects the Fermi surface to capture the nontrivial band topology[8,28] and also impacts the low-energy properties like superconductivity.[29] Thus, the superconductivity with a high SOC strength and the possible nontrivial topological band structure may direct unconventionality in the superconducting ground state. As SOC is directly proportional to the fourth power of atomic number Z, introducing a heavier element will increase the SOC strength of the system.

We have synthesized single crystals of a new member of the Bi compound family, Bi_2PdPt in this prospect. Powder XRD and Laue diffraction were performed to investigate the crystal structure and orientation. The superconducting and normal state properties of Bi_2PdPt are studied using transport, magnetization and specific heat measurements. Type-II superconductivity in the moderate coupling limit is established in Bi_2PdPt.

II. Experimental details

Single-crystals of Bi_2PdPt were prepared by the modified Bridgman method. First, the polycrystalline sample was prepared using the solid state reaction method by taking a stoichiometric mixture of the required elemental powder Bi (99.99%), Pd (99.95%) and Pt (99.9%). Subsequently, the palletized form of

Department of Physics, Indian Institute of Science Education and Research Bhopal, Bhopal, 462066, India. E-mail: rpsingh@iiserb.ac.in

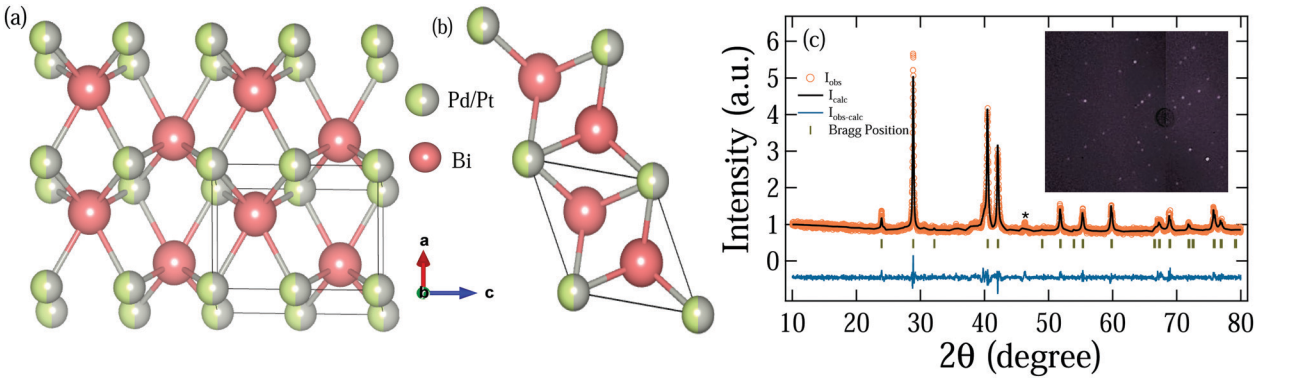

Fig. 1 NiAs hexagonal crystal structure of Bi_2PdPt is shown with solid orange balls as Bi atoms and half green or grey solid balls as Pd/Pt atoms. (a) Side view of the crystal structure and (b) top view of the crystal structure. (c) Rietveld refined pattern, represented by black lines, of XRD recorded at room temperature (open orange circles) for Bi_2PdPt. The inset shows the Laue diffraction pattern of the single-crystal.

the mixture was heated at 700 °C for four days in a vacuum-sealed tube, which was then transferred to a conical end quartz ampoule for single-crystal growth. The ampoule was kept at 700 °C for 12 h and slowly cooled to 650 °C at a rate of 0.4 °C h^{-1}, followed by water quenching. The obtained single-crystals were extremely brittle with a metallic lustre. Mechanically cleaved single-crystals were used for all of the measurements. Powder X-ray diffraction (XRD) data for the ground single crystal were collected at room temperature using a PANalytical X'Pert powder diffractometer with Cu K_α (λ = 1.5406 Å) radiation. The Laue diffraction pattern was recorded using a Photonic–Science Laue camera system for single-crystal orientation and quality determination. Magnetic measurements were performed using a Superconducting Quantum Interference Device (SQUID) of the Quantum Design Magnetic Property Measurement System (MPMS-3). AC transport and specific heat measurements were performed using the two-τ relaxation method using a Quantum Design Physical Property Measurement System (PPMS) 9 T with an applied magnetic field parallel to the crystallographic [001] axis.

III. Results and discussion

a. Sample characterization

The Rietveld refinement of the powder X-ray diffraction pattern of Bi_2PdPt was performed using the FullProf software (shown in Fig. 1).[30] A small elemental impurity peak of Pt is observed, shown by an asterisk in Fig. 1. The refined pattern confirms the crystallization of Bi_2PdPt in the NiAs hexagonal crystal structure having space group $P6_3/mmc$, which is in accordance with the literature[31] and different from the structures reported for other superconducting compounds of the family, α-BiPd (non-centrosymmetric) and α-, β-$PdBi_2$, and $PtBi_2$ (layered structures).[15,19,23,26]

The structure of Bi_2PdPt consists of Bi atoms that lie inside the hexagonal geometry while Pd and Pt atoms share the edge sites with equal probability, as shown in Fig. 1(a) and (b). Detailed refinement results with the associated Wyckoff position of each atom are summarized in Table 1. The Laue diffraction pattern of different crystals of the same batch depicts the orientation of the crystal along the [001] direction, and bright spots reveal the quality of the single-crystal, as shown in the inset of Fig. 1(c).

Table 1 Structure parameters of Bi_2PdPt obtained from the Rietveld refinement of XRD

Structure				Hexagonal	
Space group				$P6_3/mmc$	
Lattice parameters					
$a = b$(Å)				4.294(5)	
c (Å)				5.567(1)	
Atom	Wyckoff position	x	y	z	Occupancy
Bi	2c	0.333	0.666	0.250	1.0008
Pd	2a	0	0	0	0.5017
Pt	2a	0	0	0	0.4877

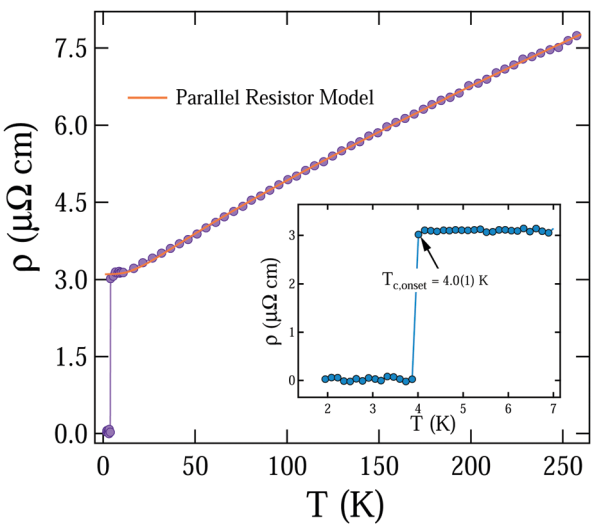

Fig. 2 Temperature dependence of resistivity in the zero field fitted above the transition temperature is shown in the main panel. The inset shows the limited temperature region presenting the superconducting transition at $T_{C,onset}$ = 4.0(1) K.

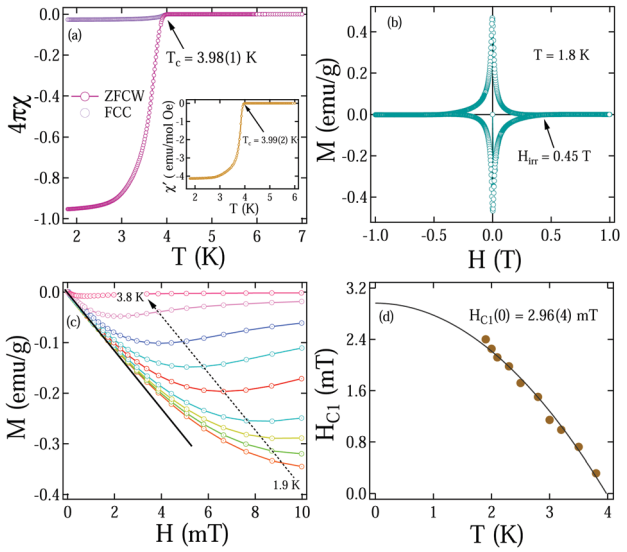

Fig. 3 (a) Superconducting transition in a 1 mT magnetic field at T_C = 3.98(1) K and the inset shows the AC susceptibility curve with the same transition temperature. (b) Magnetization hysteresis loop at 1.8 K. (c) Magnetic moment variation under a magnetic field at different temperatures up to the transition temperature. (d) The lower critical field with temperature is fitted using the GL eqn (4).

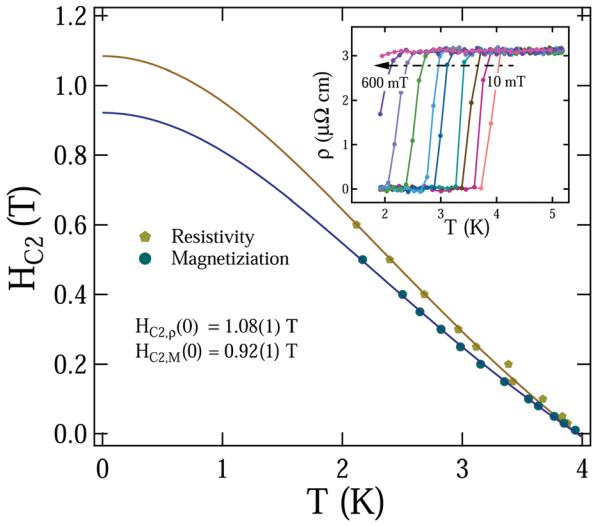

Fig. 4 The upper critical field variation with temperature (determined *via* magnetization and resistivity measurements) fitted using eqn (4) is shown. The inset shows the resistivity drop temperature variation with an applied magnetic field.

b. Superconducting and normal state properties

The in-plane AC resistivity at zero magnetic field in the temperature range of 1.9 K to 250 K was measured for the single-crystal of Bi_2PdPt, as shown in Fig. 2. A sharp resistivity drop from the normal state resistivity at $T_{C,onset}$ = 4.0(1) K with a width of 0.1 K is recorded as a superconducting transition. Above the transition temperature, the resistivity behaviour of Bi_2PdPt shows a slight deviation from the linear behaviour, which is described by Wilson's theory.[32] However, the high value of the absolute resistivity with a saturated trend is consistent with those of α-BiPd and other A15 compounds where the parallel resistor model is implanted.[33] Hence, the resistivity behaviour of Bi_2PdPt is characterized using the parallel resistor model described by Wisemann as[34]

$$\frac{1}{\rho(T)} = \frac{1}{\rho_s} + \frac{1}{\rho_i(T)} \quad (1)$$

where ρ_s is the saturated resistivity independent of the temperature and ρ_i (T) is the ideal contribution consisting of two terms which are expressed as

$$\rho_i(T) = \rho_{i,0} + C\left(\frac{T}{\Theta_R}\right)^n \int_0^{\Theta_R/T} \frac{x^n}{(e^x-1)(1-e^{-x})}\mathrm{d}x. \quad (2)$$

here, the first term $\rho_{i,0}$ is the temperature-independent residual resistivity, and the second term represents the temperature dependent contribution including the effect of electron–phonon scattering stated by the generalized Bloch–Grüneisen expression.[32,35] Θ_R is the Debye temperature from the resistivity measurement and C is a material-dependent quantity. The best fitting of Bi_2PdPt for n = 3 yield Debye temperature Θ_R = 123(3) K, C = 5.70(2) μΩ cm, ρ_s = 47(3) μΩ cm and $\rho_{i,0}$ = 3.32(1) μΩ cm. The estimated residual resistivity ratio, ρ (250 K)/ρ (5 K) = 2.5, is much smaller than the reported values for the other Bi–Pd compounds, which can be possibly due to the increase in the disorder of the system due to the presence of Pt.[33,36]

Magnetization *versus* temperature measurement under 1 mT magnetic field in zero field cooled warming (ZFCW) and field cooled cooling (FCC) modes is shown in Fig. 3(a). The curve shows a diamagnetic onset at temperature, T_C = 3.98(1) K perpendicular to the crystallographic axis [001] of single-crystal Bi_2PdPt. The poor overlap of ZFCW and FCC curves depicts the presence of strong pinning centres in the sample, and a superconducting volume fraction close to 96% from ZFCW curve certain the bulk superconducting property. The AC susceptibility results also depict the transition temperature to be 3.99(2) K in a similar magnetic field (shown in inset of Fig. 3(a)). A magnetization hysteresis loop under an applied magnetic field of ± 1 T at a temperature of 1.8 K is shown in Fig. 3(b). The loop represents the conventional type-II superconductor behaviour along with an irreversible nature of magnetization up to H_{irr} = 0.45 T, above which unpinning of the vortices starts.

Furthermore, to estimate the lower critical field value H_{C1}, the magnetization variation in the applied magnetic field at different isotherms up to the transition temperature T_C were analyzed. H_{C1} for each isotherm is considered as a magnetic field value where the curve starts to deviate from the linear Meissner state, as shown in Fig. 3(c). The temperature evolution of the lower critical field is fitted with the Ginzburg–Landau (GL) equation

$$H_{C1}(T) = H_{C1}(0)\left[1 - \left(\frac{T}{T_C}\right)^2\right] \quad (3)$$

which gives $H_{C1}(0)$ = 2.96(4) mT for T_C = 3.98(1) K (Fig. 3(d)). The upper critical field, H_{C2}, is evaluated by the observed shifts

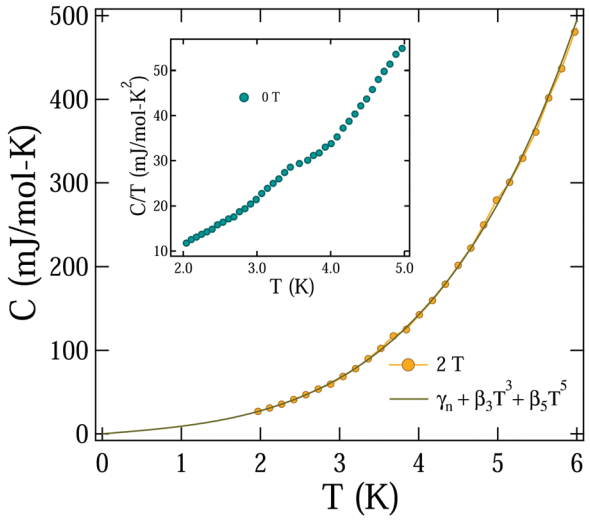

Fig. 5 Temperature dependence specific heat of Bi_2PdPt represented in the *C vs. T* form at a 2 T magnetic field is fitted with eqn (5). The inset presents the *C vs. T* curve at a zero magnetic field where an anomaly is clearly observed.

in the superconducting transition temperature with increasing applied magnetic field. The change in the transition temperature T_C is marked from magnetization at onset and for resistivity measurements at 90% drop from the normal state resistivity value ($T_{C,90\%}$), as shown in the inset of Fig. 4. The upper critical field, $H_{C2}(0)$, is estimated from the expression

$$H_{C2}(T) = H_{C2}(0)\left[\frac{(1-t^2)}{(1+t^2)}\right]. \quad (4)$$

Here $t = T/T_C$ is the reduced temperature. The fitted data yield $H_{C2,M}(0) = 0.92(1)$ T and $H_{C2,\rho}(0) = 1.08(1)$ T from magnetization and resistivity measurements, respectively, as displayed in Fig. 4.

In addition to the resistivity and magnetization measurements, the specific heat is also measured for Bi_2PdPt at zero field and 2 T (well above the upper critical field) under temperature variation, as shown in Fig. 5. A small anomaly in 0 T specific heat measurement is observed around 3.93(7) K, as shown in the inset of Fig. 5, which is consistent with the observed superconducting transition temperature from the resistivity and magnetization measurements. The measurement recorded at 2 T presents the normal state of Bi_2PdPt. The normal state specific data are fitted using the Debye relationship

$$C = \gamma_n T + \beta_3 T^3 + \beta_5 T^5 \quad (5)$$

where γ_n is the Sommerfeld coefficient corresponding to electronic contribution, β_3 is the Debye constant representing the phononic contribution, and β_5 includes the anharmonic contribution to the specific heat. The fitted data produce γ_n = 5.1(6) mJ mol^{-1} K^{-2}, β_3 = 1.72(6) mJ mol^{-1} K^{-4} and β_5 = 11.2(1) μJ mol^{-1} K^{-6} (Fig. 5). The Sommerfeld coefficient value of Bi_2PdPt matches well with the reported value of α-PdBi, but a large deviation from α- and β-$PdBi_2$ is observed.[33,36,37] According to free electron theory, the Sommerfeld coefficient is used to evaluate the density of state at the Fermi level as per the relationship $\gamma_n = \left(\frac{\pi^2 k_B^2}{3}\right) D_C(E_F)$, where $k_B = 1.38 \times 10^{-23}$ J K^{-1} is the Boltzmann constant. $D_C(E_F)$ is calculated to be 2.1(2) states eV^{-1} f.u.$^{-1}$. Furthermore, considering the Debye model, the Debye temperature Θ_D is estimated to be 165(2) K for β_3 = 1.72(6) mJ mol^{-1} K^{-4} using the expression $\theta_D = \left(\frac{12\pi^4 RN}{5\beta_3}\right)^{\frac{1}{3}}$, where R = 8.314 J mol^{-1} K^{-1} is a gas constant. The calculated Debye temperature value is consistent with the value obtained using the parallel resistor model. The average electron–phonon coupling constant, λ_{e-ph} is also calculated by implanting McMillan's theory given as[38]

$$\lambda_{e-ph} = \frac{1.04 + \mu^* \ln(\theta_D/1.45T_C)}{(1-0.62\mu^*)\ln(\theta_D/1.45T_C) - 1.04} \quad (6)$$

where μ^* varies in the range of $0.1 \leq \mu^* \leq 0.15$, a material-specific value accounting for the screened Coulomb repulsion. Considering T_C = 3.93(7) K, θ_D = 165(2) K and μ^* = 0.1 (as speculated for Bi–Pd binary compounds) λ_{e-ph} = 0.64(1) is obtained, which puts Bi_2PdPt in the moderately coupled superconductor regime respective to other Bi–Pd compounds α-, β-$PdBi_2$, and α-PdBi.[33,37]

c. Superconducting parameters and Uemura plot

The external applied magnetic field imposes a limiting field on the superconductor, portrayed independently by the spin paramagnetic and orbital limiting effects. According to the BCS theory, the spin paramagnetic effect comes from pair breaking due to the Zeeman effect defined as the Pauli limiting field, $H_{C2}^P(0) = 1.86\ T_C$.[39,40] For Bi_2PdPt with T_C = 3.98(1) K, $H_{C2}^P(0)$ = 7.40(2) T is yielded. Whereas, the orbital limit for an upper critical field refers to the critical field where vortex cores begin to overlap. The orbital limiting field is given by the Werthamer–Helfand–Hohenberg (WHH) expression[41,42]

$$H_{C2}^{orbital}(0) = -\alpha T_C \left.\frac{dH_{C2}(T)}{dT}\right|_{T=T_C} \quad (7)$$

where α = 0.69 for the dirty limit and 0.73 for the clean limit superconductors. The initial slope $\frac{-dH_{C2}(T)}{dT}$ at $T = T_C$ is estimated to be 0.23(1) T/K which gives $H_{C2}^{orbital}(0)$ = 0.64(1) T considering the dirty limit. Furthermore, the relative strength of Pauli and the orbital limiting field is measured from the Maki parameter defined using the relationship $\alpha_M = \sqrt{2}H_{C2}^{orbital}(0)/H_{C2}^P(0)$, which evaluates α_M = 0.12(2).[43] The small value of the Maki parameter indicates negligible effect of the Pauli limiting field for Bi_2PdPt.

Furthermore, the fundamental superconducting length parameters are calculated from the upper, $H_{C2}(0)$, and lower, $H_{C1}(0)$, critical field values. The Ginzburg–Landau coherence length ($\xi_{GL}(0)$) is estimated from $\xi_{GL}(0) = \sqrt{\frac{\Phi_0}{2\pi H_{C2}(0)}}$,[44] where $\Phi_0 = 2.07 \times 10^{-15}$ T m^2 is the magnetic flux quantum. Using $H_{C2,M}(0)$ = 0.92(1) T, $\xi_{GL}(0)$ is evaluated as 190(1) Å.

The equation[45]

$$H_{C1}(0) = \frac{\Phi_0}{4\pi\lambda_{GL}^2(0)}\left(\ln\frac{\lambda_{GL}(0)}{\xi_{GL}(0)} + 0.12\right) \quad (8)$$

provides the Ginzburg–Landau penetration depth, $\lambda_{GL}(0)$ = 4231(76) Å, for $H_{C1}(0)$ = 2.96(4) mT and $\xi_{GL}(0)$ = 190(1) Å. Moreover, the ratio $\frac{\lambda_{GL}(0)}{\xi_{GL}(0)}$ gives the Ginzburg–Landau parameter, κ_{GL} = 22.2(5), which is much higher than $1/\sqrt{2}$, indicating a strong type-II superconductivity in Bi_2PdPt. The thermodynamic critical field, H_C, is evaluated using the expression:[45] $H_{C1}(0)\,H_{C2}(0) = H_C^2 \ln\kappa_{GL}$, yielding H_C = 29(1) mT.

For Bi_2PdPt, to determine the rest of the superconducting parameters including the London penetration depth, λ_L, and the electronic mean free path, l_e, and to verify the dirty limit superconductivity, a set of equations is used assuming the spherical Fermi surface. The electronic mean free path, l_e, is estimated from the quasiparticle number density, n, and Sommerfeld coefficient, γ_n. The quasiparticle number density of Bi_2PdPt has been extracted from the Hall measurement, n = 2.45(2) × 10^{28} m^{-3} (more details are provided in the Appendix). The Fermi vector, k_F, is evaluated using $k_F = (3\pi^2 n)^{1/3}$, which gives k_F = 0.90(1) $Å^{-1}$. The effective mass, m^*, is calculated from the Sommerfeld coefficient *via* relation, $m^* = (\hbar k_F)^2\gamma_n/\pi^2 n k_B^2$, where k_B is the Boltzmann constant, γ_n = 95.51 J m^{-3} K^{-2} and m^* = 2.0(3) m_e. According to the Drude model,[44] the Fermi velocity is determined from the relationship $v_F = \hbar k_F/m^*$ = 5.1(7) × 10^5 m s^{-1} and scattering time is determined from $\tau^{-1} = ne^2\rho_0/m^*$, which was further used to calculate the electronic mean free path, $l_e = v_F\tau$, providing l_e = 455(68) Å.

In consideration of BCS theory, the coherence length ξ_0 is defined as $0.18\hbar v_F/k_B T_C$ providing ξ_0 = 1756(147) Å. A ξ_0/l_e ratio of 3.9 is greater than 1, implying that Bi_2PdPt is a dirty limit superconductor. Furthermore, in the dirty limit, the London penetration depth, λ_L,[46] is written as

$$\lambda_L = \left(\frac{m^*}{\mu_0 n e^2}\right)^{1/2}. \quad (9)$$

From the above expression the estimated λ_L is 483(36) Å. The order of calculated parameters matches well with β-$PdBi_2$ where the dirty limit superconductivity is observed[24] whereas α-PdBi lies in the clean type-II superconducting limit.[33]

Moreover, to classify Bi_2PdPt in the context of other superconductors, the Uemura plot[47] of T_C with the effective Fermi temperature, T_F, has been plotted, which is used to define the unconventionality characteristics of a superconductor based on the $\frac{T_C}{T_F}$ ratio. For the 3D spherical Fermi surface, the Fermi temperature is calculated using[48]

$$k_B T_F = \frac{\hbar^2}{2}(3\pi^2)^{2/3}\frac{n^{2/3}}{m^*}, \quad (10)$$

where n is the quasiparticle number density per unit volume, and m^* is the effective mass of quasiparticles. The T_F value is estimated to be T_F = 17576 (104) K, considering the respective values of the parameters from Table 2. The ratio $\frac{T_C}{T_F}$ = 0.0002 places this material, Bi_2PdPt, close to the other family member, β-$PdBi_2$, and outside the band of the unconventional superconductor which includes iron based superconductors, cuprates and Chevrel phase.[49,50] Conventional superconductors are considered to be on the right-hand side of the Uemura plot. Bi_2PdPt with the other member of the Bi–Pd compound family, β-$PdBi_2$,[24] is shown by the solid green symbol in Fig. 6.

Table 2 Parameters in the superconducting and normal states of Bi_2PdPt and α-BiPd

Parameters	Unit	Bi_2PdPt	α-BiPd[33]
T_C	K	4.0	3.8
H_{C1} (0)	mT	2.96	12.0
$H_{C2,M}$ (0)	T	0.92	0.8
H_{C2}^{P} (0)	T	7.40	7.07
$H_{C2}^{Orbital}$ (0)	T	0.64	
ξ_{GL} (0)	Å	190	170
λ_{GL} (0)	Å	4231	1792
k_{GL}		22.2	7.6
γ_n	mJ mol^{-1} K^{-2}	5.1	4.0
θ_D	K	165.0	169.0
ξ_0/l_e		3.9	0.01
v_F	10^5 m s^{-1}	5.1	
n	10^{28} m^{-3}	2.45	
T_F	K	17576	
m^*/m_e		2.0	

Among the Bi–Pd compound family, Bi_2PdPt is a possible high SOC candidate, based on the presence of heavy constituent elements establishing a strong foundation to exhibit intriguing properties. The different crystal structure NiAs type of Bi_2PdPt eliminates all the possibilities of the presence of any secondary superconducting phase of the Bi–Pd/Pt compound, implementing

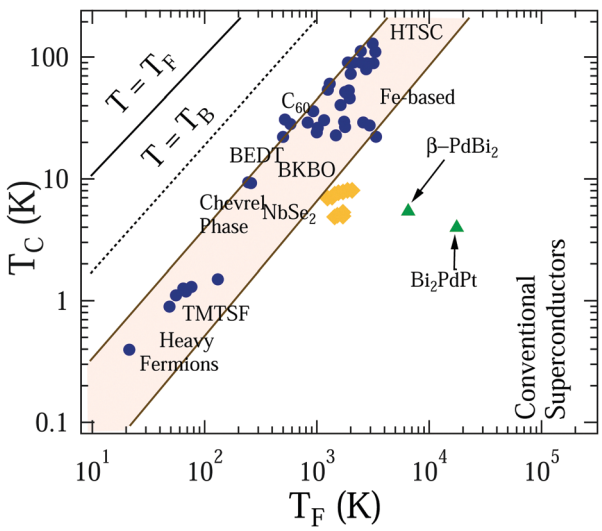

Fig. 6 Uemura plot showing the superconducting transition temperature T_C *vs.* the effective Fermi temperature T_F for Bi_2PdPt with β-$PdBi_2$, shown as solid green triangles. Other data points represent the different families of superconductors together with the shaded region representing the families of unconventional superconductors. The dashed line corresponds to the Bose–Einstein condensation temperature T_B.

intrinsic bulk superconductivity. The recorded superconducting transition temperature of 4.0 K for Bi_2PdPt is close to that for α-BiPd though both have different crystal structures. Furthermore, the Hall measurement (see the Appendix) suggests dominated hole charge carriers (10^{28} m^{-3}) the same as for other Bi–Pd compounds, which indicate negligible effect of Pt on the electronic states. The specific heat of Bi_2 PdPt gives a Sommerfeld coefficient of 5.1(6) mJ mol^{-1} K^{-2}, which is slightly higher than what is reported for α-BiPd (4.0 mJ mol^{-1} K^{-2}), suggesting only a minimal increase in the density of states at E_F. However, the observed value is comparable to those of β-$PdBi_2$ and $Pt_{1.26}Bi_2$.[51] Concluding that neither substitution at the Pd site nor increasing the Bi concentration predominately affects the density of states in Bi–Pd/Pt compounds. Despite the presence of a heavy 5d Pt element, no change in phonon frequency, extracted from the Debye temperature, is noted between Bi_2PdPt and α-BiPd.[33]

Moreover, the present bulk measurement of Bi_2PdPt is not sufficient to establish the gap symmetry of the sample. The possible explanation for a low specific jump value can be due to multiband superconductivity with a single superconducting gap.[52] Also, layered transition-metal dichalcogenide superconductors are well known to exhibit no anomaly in specific heat measurement.[53] In addition, the low value of specific heat jump or no jump at all has been observed in many Bi-based half-Heusler alloys (RPdBi), where superconductivity is attributed to surface states.[54] Furthermore, the similar behaviour is determined in the case of strongly or locally disordered systems such as quasi-skutterudites.[55]

No deviation or anisotropy has been observed in the upper critical field of Bi_2PdPt, directing toward the bulk nature of the superconducting state and the absence of multigap superconductivity. Apart from this, the variation of the superconducting volume fraction with the different cooling procedures of sample preparation showed the disorder effect in the sample (details are provided in the Appendix). To fully understand the effect of increased SOC strength, the possible reason for the low value of the specific heat jump and the presence of the nontrivial band structure in Bi_2PdPt detailed theoretical and experimental analyses of the superconducting ground state with band topology are required.

IV. Conclusions

In summary, we synthesized single-crystal Bi_2PdPt and transport, magnetization, and specific heat measurements were performed for the detailed analysis of superconducting properties. The superconducting transition of Bi_2PdPt has been recorded at 4.0(1) K with upper and lower critical field values, $H_{C1}(0)$ = 2.96(4) mT and $H_{C2,M}(0)$ = 0.92(1) T, fitted using the Ginzburg–Landau equation. An anomaly is observed around the transition temperature in specific heat measurement, confirming the bulk superconductivity. The comparison of various normal and superconducting state parameters of Bi_2 PdPt and α-BiPd is summarized in Table 2. Bi_2PdPt is classified as a moderately coupled type-II dirty limit superconductor. The estimated value of the Fermi temperature T_F places Bi_2PdPt close to the other member of the family, β-$PdBi_2$ in the Uemura plot. Further microscopy measurements such as muon spectroscopy, scanning tunneling microscopy (STM) and angle-resolved photoemission spectroscopy (ARPES) are required to understand the superconducting ground state and the possible topological nature of Bi_2PdPt.

Conflicts of interest

The authors declare no conflicts of interest.

Appendix

a. Characterization

The superconducting volume fraction in Bi_2PdPt is highly dependent on the sample cooling procedure during preparation. Three different samples were made such as S1 cooled at 1.0 °C h^{-1}, S2 cooled at 0.5 °C h^{-1}, and S3 cooled at 0.4 °C h^{-1} while preparing the sample. XRD patterns of the two samples S2 and S3 are shown in Fig. 7(a). The results of the magnetic characterization of S1 and S2 are presented in Fig. 7(b). The observed superconducting transition temperature is the same for all three samples; however, the superconducting shielding fraction 96% is the maximum for S3. S2 only shows 60% volume fraction with less than 10% fraction observed in S1, implying that samples cooled only at a specific rate show a large volume fraction with the same diamagnetic onset temperature in magnetization measurement. This variation of superconducting fraction reflects the effect on grain boundaries,

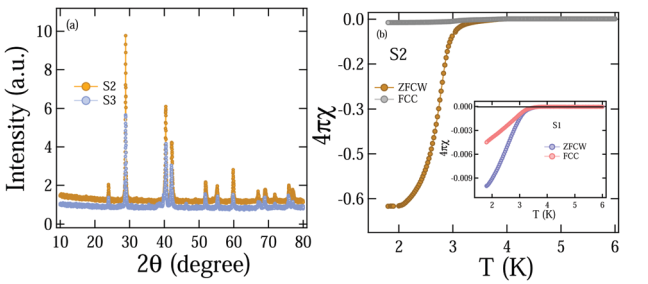

Fig. 7 (a) XRD comparison of the powder sample having two different cooling rates of 0.5 °C h^{-1} (S2) and 0.4 °C h^{-1} (S3) during preparation. (b) Magnetic measurement compilation of S2 and S1 in the inset, whereas S3 is shown in Fig. 3(a).

Table 3 Elemental concentration obtained from the EDS measurements at 3 different positions

Elements	Bi	Pt	Pd
Atm%			
Scan 1	45.9	24.0	30.1
Scan 2	44.6	26.5	28.9
Scan 3	46.5	24.1	29.4

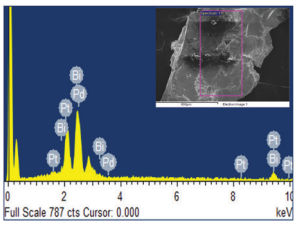

Fig. 8 EDS pattern of the Bi_2PdPt sample with the SEM image in the inset.

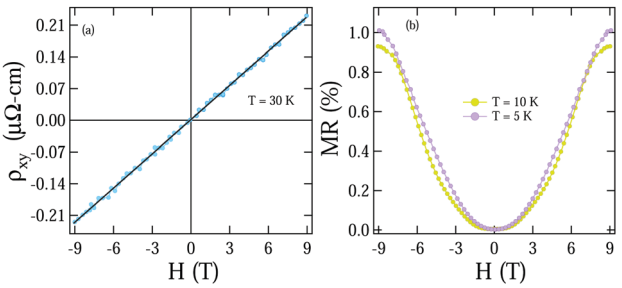

Fig. 9 (a) Hall resistivity at T = 30 K under a field variation of ±9 T. (b) MR data taken at T = 5 K and T = 10 K on the Bi_2 PdPt crystal.

disorder and point defects of samples due to different cooling procedures.[56] The energy dispersive spectroscopy (EDS) analysis for Bi_2PdPt is summarised in Table 3, stating the nominal composition within the error limit, and the corresponding spectra is also shown in the inset of Fig. 8.

b. Normal state properties

To perceive the normal state properties of Bi_2PdPt, magnetoresistance (MR) and normal Hall effects were also measured. Hall measurements were performed on Bi_2PdPt under a varying magnetic field of ±9 T at 30 K to extract the carrier density as shown in the left panel of Fig. 9(a), where a linear variation with the magnetic field represents the small contribution of the longitudinal resistivity. The Hall coefficient, R_H, was determined by the slope of the variation ρ_{xy} with both +H and −H fields. The estimated R_H is $2.52(2) \times 10^{-4}$ cm^3 C^{-1}, and the positive sign indicates the hole as the dominant charge carrier in the sample. By simply using the single band expression $n = 1/R_H q$, the electron concentrations were calculated, $n = 2.45(2) \times 10^{28}$ m^{-3}. The carrier density order matches well with those reported for α-PdBi and $PdBi_2$.[57] MR was measured in the longitudinal configuration under a varying magnetic field of 9 T at different temperatures. The magnetic field dependence MR is defined as $\frac{\rho_{xx}(H) - \rho_{xx}(0)}{\rho_{xx}(0)}$. A significant small MR value is observed in our sample Fig. 9(b).

Acknowledgements

A. Kataria acknowledges the funding agency Council of Scientific and Industrial Research (CSIR), Government of India, for providing the SRF fellowship (Award No: 09/1020(0172)/2019-EMR-I). R. P. S. acknowledges the Science and Engineering Research Board, Government of India, for the Core Research Grant CRG/2019/001028.

References

1 A. P. Schnyder, S. Ryu, A. Furusaki and A. W.-W. Ludwig, *Phys. Rev. B: Condens. Matter Mater. Phys.*, 2008, **78**, 195125.
2 X. L. Qi, T. L. Hughes, S. Raghu and S. C. Zhang, *Phys. Rev. Lett.*, 2009, **102**, 187001.
3 X. L. Qi and S. C. Zhang, *Rev. Mod. Phys.*, 2011, **83**, 1057.
4 M. Sato and Y. Ando, *Rep. Prog. Phys.*, 2017, **80**, 076501.
5 L. Fu and C. L. Kane, *Phys. Rev. Lett.*, 2008, **100**, 096407.
6 A. Yu. Kitaev, *Phys.-Usp.*, 2001, **44**, 131.
7 L. Fu and C. L. Kane, *Phys. Rev. B: Condens. Matter Mater. Phys.*, 2007, **76**, 045302.
8 H. Zhang, C. X. Liu, X. L. Qi, X. Dai, Z. Fang and S. C. Zhang, *Nat. Phys.*, 2009, **5**, 438.
9 T. Sato, K. Segawa, H. Guo, K. Sugawara, S. Souma, T. Takahashi and Y. Ando, *Phys. Rev. Lett.*, 2010, **105**, 136802.
10 K. Kuroda, M. Ye, A. Kimura, S. V. Eremeev, E. E. Krasovskii, E. V. Chulkov, Y. Ueda, K. Miyamoto, T. Okuda, K. Shimada, H. Namatame and M. Taniguchi, *Phys. Rev. Lett.*, 2010, **105**, 146801.
11 Y. L. Chen, Z. K. Liu, J. G. Analytis, J.-H. Chu, H. J. Zhang, B. H. Yan, S.-K. Mo, R. G. Moore, D. H. Lu, I. R. Fisher, S. C. Zhang, Z. Hussain and Z.-X. Shen, *Phys. Rev. Lett.*, 2010, **105**, 266401.
12 S. Souma, K. Eto, M. Nomura, K. Nakayama, T. Sato, T. Takahashi, K. Segawa and Y. Ando, *Phys. Rev. Lett.*, 2012, **108**, 116801.
13 K. Kuroda, H. Miyahara, M. Ye, S. V. Eremeev, Yu.-M. Koroteev, E. E. Krasovskii, E. V. Chulkov, S. Hiramoto, C. Moriyoshi, Y. Kuroiwa, K. Miyamoto, T. Okuda, M. Arita, K. Shimada, H. Namatame, M. Taniguchi, Y. Ueda and A. Kimura, *Phys. Rev. Lett.*, 2012, **108**, 206803.
14 Y. Nakajima, R. Hu, K. Kirshenbaum, A. Hughes, P. Syers, X. Wang and J. Paglione, *Sci. Adv.*, 2015, **1**, e1500242.
15 Y. Zhou, X. Chen, C. An, Y. Zhou, L. Ling, J. Yang, C. Chen, L. Zhang, M. Tian, Z. Zhang and Z. Yang, *Phys. Rev. B: Condens. Matter Mater. Phys.*, 2019, **99**, 054501.
16 S. Mitra, K. Okawa, S. K. Sudheesh, T. Sasagawa, J.-X. Zhu and E. E.-M. Chia, *Phys. Rev. B: Condens. Matter Mater. Phys.*, 2017, **95**, 134519.
17 K. Dimitri, M. M. Hosen, G. Dhakal, H. Choi, F. Kabir, C. Sims, D. Kaczorowski, T. Durakiewicz, J. X. Zhu and M. Neupane, *Phys. Rev. B: Condens. Matter Mater. Phys.*, 2018, **97**, 144514.
18 H. Choi, M. Neupane, T. Sasagawa, E. E.-M. Chia and J. X. Zhu, *Phys. Rev. Mater.*, 2017, **1**, 034201.
19 Z. Sun, M. Enayat, A. Maldonado, C. Lithgow, E. Yelland, D. Peets, D. C. Peets, A. Yaresko, A. P. Schnyder and P. Wahl, *Nat. Commun.*, 2015, **6**, 1.
20 A. Yaresko, A. P. Schnyder, H. M. Benia, C. M. Yim, G. Levy, A. Damascelli, C. R. Ast, D. C. Peets and P. Wahl, *Phys. Rev. B: Condens. Matter Mater. Phys.*, 2018, **97**, 075108.

21 M. Sakano, K. Okawa, M. Kanou, H. Sanjo, T. Okuda, T. Sasagawa and K. Ishizaka, *Nat. Commun.*, 2015, **6**, 8595.
22 T. Xu, B. T. Wang, M. Wang, Q. Jiang, X. P. Shen, B. Gao, M. Ye and S. Qiao, *Phys. Rev. B: Condens. Matter Mater. Phys.*, 2019, **100**, 161109(R).
23 J. Kacmarcik, Z. Pribulova, T. Samuely, P. Szabo, V. Cambel, J. Soltys, E. Herrera, H. Suderow, A. Correa-Orellana, D. Prabhakaran and P. Samuely, *Phys. Rev. B: Condens. Matter Mater. Phys.*, 2016, **93**, 144502.
24 P. K. Biswas, D. G. Mazzone, R. Sibille, E. Pomjakushina, K. Conder, H. Luetkens, C. Baines, J. L. Gavilano, M. Kenzelmann, A. Amato and E. Morenzoni, *Phys. Rev. B: Condens. Matter Mater. Phys.*, 2016, **93**, 220504(R).
25 E. Herrera, I. Guillamon, J. A. Galvis, A. Correa, A. Fente, R. F. Luccas, F. J. Mompean, M. Garcia-Hernandez, S. Vieira, J. P. Brison and H. Suderow, *Phys. Rev. B: Condens. Matter Mater. Phys.*, 2015, **92**, 054507.
26 C. Q. Xu, X. Z. Xing, X. Xu, B. Li, B. Chen, L. Q. Che, X. Lu, J. Dai and Z. X. Shi, *Phys. Rev. B: Condens. Matter Mater. Phys.*, 2016, **94**, 165119.
27 J. Wang, X. Chen, Y. Zhou, C. An, Y. Zhou, C. Gu, M. Tian and Z. Yang, *Phys. Rev. B: Condens. Matter Mater. Phys.*, 2021, **103**, 014507.
28 M. Z. Hasan and C. L. Kane, *Rev. Mod. Phys.*, 2010, **82**(4), 3045.
29 D. F. Shao, X. Luo, W. J. Lu, L. Hu, X. D. Zhu, W. H. Song, X. B. Zhu and Y. P. Sun, *Sci. Rep.*, 2016, **6**, 1.
30 J. Rodríguez-Carvajal, *Phys. B*, 1993, **192**, 55.
31 N. N. Zhuravlev, G. S. Zhdanov and Y. M. Smirnova, *Phys. Met. Metallogr.*, 1962, **13**, 55.
32 A. H. Wilson, *Theory of Metals*, Cambridge University Press, Cambridge, England, 1958.
33 B. Joshi, A. Thamizhavel and S. Ramakrishnan, *Phys. Rev. B: Condens. Matter Mater. Phys.*, 2011, **84**, 064518.
34 H. Wiesmann, M. Gurvitch, H. Lutz, A. K. Ghosh, B. Schwarz, M. Strongin, P. B. Allen and J. W. Halley, *Phys. Rev. Lett.*, 1977, **38**, 782.
35 G. Grimvall, *The Electron–Phonon Interaction in Metals*, North-Holland, Amsterdam, 1981.
36 Y. Imai, F. Nabeshima, T. Yoshinaka, K. Miyatani, R. Kondo, S. Komiya, I. Tsukada and A. Maeda, *J. Phys. Soc. Jpn.*, 2012, **81**, 113708.
37 G. Pristas, Mat Orendac, S. Gabani, J. Kacmarcik, E. Gazo, Z. Pribulova, A. Correa-Orellana, E. Herrera, H. Suderow and P. Samuely, *Phys. Rev. B: Condens. Matter Mater. Phys.*, 2018, **97**, 134505.
38 W. L. McMillan, *Phys. Rev.*, 1968, **167**, 331.
39 B. S. Chandrasekhar, *Appl. Phys. Lett.*, 1962, **1**, 7.
40 A. M. Clogston, *Phys. Rev. Lett.*, 1962, **9**, 266.
41 E. Helfand and N. R. Werthamer, *Phys. Rev.*, 1966, **147**, 288.
42 N. R. Werthamer, E. Helfand and P. C. Hohenberg, *Phys. Rev.*, 1966, **147**, 295.
43 K. Maki, *Phys. Rev. B: Condens. Matter Mater. Phys.*, 1966, **148**, 362.
44 M. Tinkham, *Introduction to Superconductivity*, McGraw-Hill, New York, 2nd edn, 1996.
45 T. Klimczuk, F. Ronning, V. Sidorov, R. J. Cava and J. D. Thompson, *Phys. Rev. Lett.*, 2007, **99**, 257004.
46 D. A. Mayoh, J. A.-T. Barker, R. P. Singh, G. Balakrishnan, D. Mc. K. Paul and M. R. Lees, *Phys. Rev. B: Condens. Matter Mater. Phys.*, 2017, **96**, 064521.
47 Y. J. Uemura, G. M. Luke, B. J. Sternlieb, J. H. Brewer, J. F. Carolan, W. N. Hardy, R. Kadono, J. R. Kempton, R. F. Kiefl, S. R. Kreitzman, P. Mulhern, T. M. Riseman, D. L. Williams, B. X. Yang, S. Uchida, H. Takagi, J. Gopalakrishnan, A. W. Sleight, M. A. Subramanian, C. L. Chien, M. Z. Cieplak, G. Xiao, V. Y. Lee, B. W. Statt, C. E. Stronach, W. J. Kossler and X. H. Yu, *Phys. Rev. Lett.*, 1989, **62**, 2317.
48 A. D. Hillier and R. Cywinski, *Appl. Magn. Reson.*, 1997, **13**, 95.
49 K. Hashimoto, K. Cho, T. Shibauchi, S. Kasahara, Y. Mizukami, R. Katsumata, Y. Tsuruhara, T. Terashima, H. Ikeda, M. A. Tanatar, H. Kitano, N. Salovich, R. W. Giannetta, P. Walmsley, A. Carrington, R. Prozorov and Y. Matsuda, *Science*, 2012, **336**, 1554.
50 R. Khasanov, H. Luetkens, A. Amato, H. H. Klauss, Z. A. Ren, J. Yang, W. Lu and Z. X. Zhao, *Phys. Rev. B: Condens. Matter Mater. Phys.*, 2008, **78**, 092506.
51 K. Kudo, H. Y. Nguyen, C. Oh, K. Takaki and M. Nohara, *J. Phys. Soc. Jpn.*, 2021, **90**, 063706.
52 E. Herrera, I. Guillamon, J. A. Galvis, A. Correa, A. Fente, R. F. Luccas, F. J. Mompean, M. Garcia-Hernandez, S. Vieira, J. P. Brison and H. Suderow, *Phys. Rev. B: Condens. Matter Mater. Phys.*, 2015, **92**, 054507.
53 M. Mandal and R. P. Singh, *J. Phys.: Condens. Matter*, 2021, **33**, 135602.
54 P. Orest, D. Kaczorowski and P. Wisniewski, *Sci. Rep.*, 2015, **5**, 1.
55 A. Slebarski, M. M. Maska, M. Fijalkowski, C. A. McElroy and M. B. Maple, *J. Alloys Compd.*, 2015, **646**, 866.
56 W. Liu, S. Li, H. Wu, N. Dhale, P. Koirala and B. Lv, *Phys. Rev. Mater.*, 2021, **5**, 014802.
57 K. Zhao, B. Lv, Y. Y. Xue, X. Y. Zhu, L. Z. Deng, Z. Wu and C. W. Chu, *Phys. Rev. B: Condens. Matter Mater. Phys.*, 2015, **92**, 174404.